THE JOURNAL OF PHYSICAL CHEMISTRY B

Article

pubs.acs.org/JPCB

Structure and Energetics of $Li^+-(BF_4^-)_n$, $Li^+-(FSI^-)_n$, and $Li^+-(TFSI^-)_n$: Ab Initio and Polarizable Force Field Approaches

Charles W. Bauschlicher, Jr.,*[,†] Justin B. Haskins,[‡] Eric W. Bucholz,[‡] and John W. Lawson[‡]

NASA Ames Research Center, Moffett Field, California 94035, United States

Oleg Borodin

Electrochemistry Branch, Sensor & Electron Devices Directorate, U.S. Army Research Laboratory, Adelphi, Maryland 20783, United States

Supporting Information

ABSTRACT: The $Li^+-BF_4^-$ and $BF_4^--BF_4^-$ interactions are studied using second order perturbation theory (MP2) and coupled cluster singles and doubles approach, including the effect of connected triples, CCSD(T). The MP2 and CCSD(T) results are in excellent agreement. Using only the MP2 approach, the interactions of Li^+ with bis(trifluoromethane)sulfonimide anion (TFSI) and Li^+ with bis(fluorosulfonyl)imide anion (FSI) are studied. The results of these high level calculations are compared with density functional theory (DFT) calculations for a variety of functionals and with the APPLE&P force field. The B3LYP approach well reproduces the accurate calculations using both a small and large basis set. The M06 and M06L functionals in the larger basis set are in good agreement with the high level calculations. While the APPLE&P force field does not outperform the best functionals, the APPLE&P results agree better with the accurate results than do some of the functionals tested.

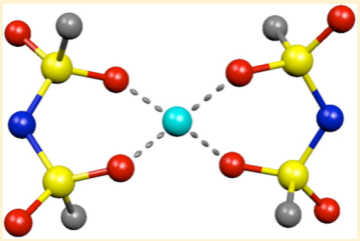

I. INTRODUCTION

Computational power has grown at astounding rates for a considerable length of time. One component of portable computing that has not shown the impressive increase is batteries. The use of lithium metal anodes offers the possibility of dramatically increasing battery performance. One critical component that is needed to make this a reality is controlling the Li dendrite growth. Recent work using ionic liquids has shown some promise in dendrite suppression.[1,2] Finding the ideal ionic liquid is a nontrivial task due to the enormous number of possible ionic liquids. Computational modeling could be very helpful in this regard; by modeling the systems that have been studied experimentally, it should be possible to understand why some ionic liquids work better than others. Using this knowledge should enable the optimal choices of systems to be studied experimentally. Such computational studies have begun using the molecular dynamics (MD) approach. The MD calculations rely on evaluating the energy of a system at many atomic positions. Since it is prohibitively expensive to evaluate the energy using accurate computational methods for each geometry in a MD simulation, a simple function of the energy is used. The function can be based on experimental and/or computational data. The accuracy of this potential function clearly determines the accuracy of the entire simulation.

In ionic liquids, the most important interactions are the charge−charge terms. However, the interaction of the ions induces a distortion or polarization of the neighboring ions. This polarization is important in accurately describing the interaction energy of ions. Therefore, it is difficult to capture the anion−cation energetics using a classical energy function. However, simulations of ionic liquids that include polarization terms in the potential have been shown[3] to be in excellent agreement with experiment. While the results obtained for pure ionic liquids are excellent, simulations including Li^+ are noticeably less accurate.[4]

In this work, we consider the interaction of Li^+ with the BF_4, FSI, and TFSI anions as a function of level of theory. We should note there have been several previous studies[4−8] of these systems, where different DFT functionals were compared with experimental infrared spectra and with more traditional ab initio methods. While we study some of the systems using the same or similar methods, our goal is to provide the best estimate possible for the binding energies of these systems and to provide a systematic assessment of the accuracy of different density functionals and the choice of basis set. This will help determine the most reliable computational approach to generate data to develop new potentials and/or to test potentials for their reliability. In particular, we assess the reliability of the atomistic polarizable potential for liquids, electrolytes, and polymers (APPLE&P) force field recently developed by Borodin and co-workers.[9] On the basis of this calibration, extensive simulations of ionic liquids for Li battery applications were performed[10] using the APPLE&P force field

Received: June 27, 2014
Revised: August 20, 2014
Published: August 21, 2014

and the results were found to be in excellent agreement with the available experimental data.

II. METHODS

Density functional theory calculations were performed using a variety of functionals. Those used include the following: the hybrid[11] B3LYP[12] functional, the B3LYP functional with the dispersion term of Grimme,[13] which we denote as B3LYP+D, the Becke exchange function[14] with the Perdew–Wang[15] correlation functional (BPW91), the Perdew–Wang exchange and correlation functional (PW91PW91), and the M05,[16] M06,[17] and M06L[18] functionals of Truhlar and co-workers. In addition, more traditional methods for accounting for electron correlation were used; these include second order Møller–Plesset perturbation theory (MP2) and coupled cluster singles and doubles approach,[19] including the effect of connected triples determined using perturbation theory,[20] CCSD(T). The results of the *ab initio* calculations are compared with those obtained using the APPLE&P force field.[9] For $LiBF_4$, we also use a modified version of this force field, which is denoted e44. The e44 force field parameters are included in the Supporting Information.

The DFT calculations are performed using the 6-31+G** set of Pople and co-workers[21] and the augmented correlation consistent polarized triple-ζ (aug-cc-pVTZ) set of Dunning and co-workers.[22,23] The MP2 and CCSD(T) calculations are performed using the aug-cc-pVTZ and quadruple and quintuple zeta analogues, aug-cc-pVQZ and aug-pV5Z, respectively. The MP2 and/or CCSD(T) calculations are extrapolated to the complete basis set limit (CBS) using the X^{-3} approach of Helgaker et al.[24] The Gaussian 09 program[25] was used for all of the calculations except those involving the APPLE&P force field, which were preformed with a modified version of LAMMPS.[26]

Unless otherwise noted, all of the geometric parameters have been fully optimized. For the ab initio techniques, the harmonic frequencies were computed to ensure that the structures correspond to minima. The binding energies reported do not include zero-point energy, since we are unable to easily obtain vibrational frequencies for the APPLE&P results.

III. RESULTS AND DISCUSSION

A. $Li^+(BF_4^-)_n$, n = 1–4. The optimized structures of $Li^+(BF_4^-)_n$, n = 1–4, are shown in Figure 1. The equilibrium geometry for the $Li^+BF_4^-$ has two F atoms pointing at the Li^+; that is, the system has a bidentate or $\eta2$ coordination, with C_{2v} symmetry. The $\eta3$ coordination is slightly (0.7 kcal/mol) less favorable than the $\eta2$, while the $\eta1$ is much less (18.3 kcal/mol) favorable; see Table 1. We should note that the $\eta1$ case is not a stationary point, having two imaginary frequencies. While the $\eta2$ and $\eta3$ structures have similar Li–B bond lengths, not surprisingly, the $\eta1$, with one F pointing at the Li^+, has a significantly longer Li–B bond distance.

Next we evaluate the $Li^+–BF_4^-$ interaction energy at the optimal Li–B bond lengths for the $\eta2$ and $\eta1$ systems. At the $\eta2$ Li–B distance, the $\eta1$ system is almost 300 kcal/mol above the $\eta2$ system, compared to 18.3 kcal/mol if each is at its own equilibrium distance. The huge decrease in the interaction energy for $\eta1$ at the shorter Li–B bond length is due to the Li–F repulsion arising from the very short Li–F distance. Of even more interest are the relative binding energies at the long $\eta1$ Li–B distance, where the $\eta1$ system is below both the $\eta2$ and $\eta3$ configurations. That is, the $\eta1$ coordination is favored at long r values.

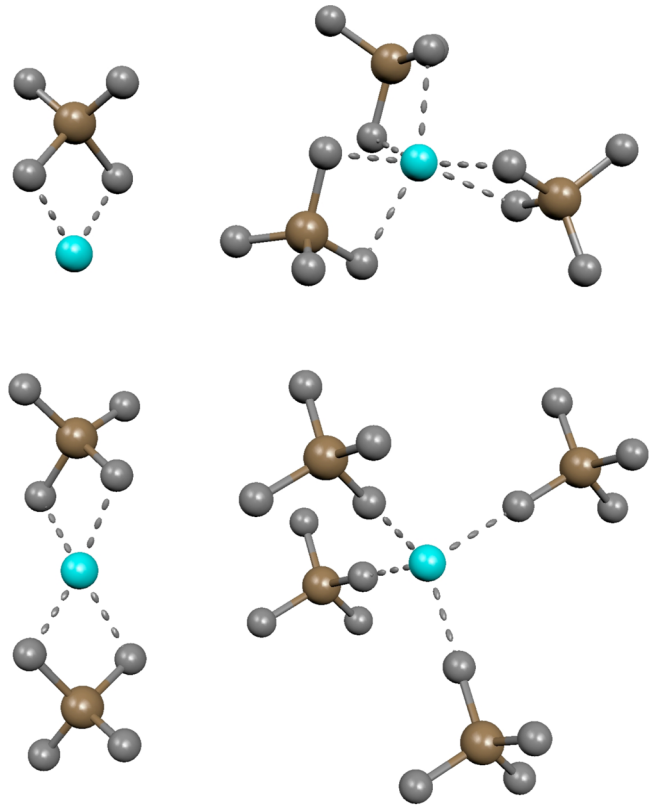

Figure 1. Optimal geometry of $Li^+(BF_4^-)_n$ species.

The equilibrium structure for $Li^+(BF_4^-)_2$ has both BF_4^- units with $\eta2$ coordination, and the two BF_4^- ligands are staggered with respect to each other, yielding D_{2d} symmetry. The energy separation between the $\eta2$ and $\eta3$ coordinations of $Li^+(BF_4^-)_2$ is more than twice that found for the analogous separation in $Li^+–BF_4^-$; see Table 1. This is due to the larger $BF_4^-–BF_4^-$ repulsion for the $\eta3$ coordination. Note that we evaluate the $BF_4^-–BF_4^-$ repulsion by removing the Li^+ and comparing the $(BF_4^-)_2$ energy with twice that of BF_4^-. Unlike the $\eta3$ coordination, the separation between the $\eta1$ and $\eta2$ coordination is very similar for the $Li^+–BF_4^-$ and $Li^+(BF_4^-)_2$ systems, 18.7 vs 18.3 kcal/mol. This arises because the $\eta1$ coordination of $Li^+(BF_4^-)_2$ has 10.9 kcal/mol less $BF_4^-–BF_4^-$ repulsion than the $\eta2$ case. The larger $BF_4^-–BF_4^-$ repulsion in the $\eta2$ case is clear from the increase in the $\eta2$ bond length when the second BF_4^- is added. This increase in bond length reduces the electrostatic interaction by about 5 kcal/mol. Since the $\eta1$ has a much longer bond length, the repulsion is smaller than that for the $\eta2$ and not surprisingly the Li–B distance does not change significantly when the second BF_4^- is added.

The equilibrium structure for $Li^+(BF_4^-)_3$ has all three BF_4^- units with $\eta2$ coordination. Compared with $Li^+(BF_4^-)_2$, the three ligands undergo a rotation about the Li–B axis to reduce the $BF_4^-–BF_4^-$ repulsion, which results in D_3 symmetry. We found a structure with two $\eta2$ and one $\eta1$ coordination to be only 1 kcal/mol higher in energy. As shown in Table 1, this mixed case has a smaller $BF_4^-–BF_4^-$ repulsive energy, but the reduced repulsion is not sufficient to overcome the more favorable $Li^+–BF_4^-$ interaction associated with $\eta2$. Also, note that the Li–B distance increases by much more for the $\eta2$ configuration when the third ligand is added, which reduces the

dx.doi.org/10.1021/jp506422p | J. Phys. Chem. B 2014, 118, 10785–10794

Table 1. Summary of $Li^+(BF_4^-)_n$, n = 1−4, B3LYP+D/6-31+G** Calculations[a]

	r_e(Li−B)					
one BF_4	$\eta2$	$\eta3$	$\eta1$	$\Delta E(r_e)$[b]	$\Delta E(\eta2\ r_e)$[c]	$\Delta E(\eta1\ r_e)$[d]
$\eta2$	2.37			0.0	0.0	0.0
$\eta3$		2.20		0.7	11.8	7.1
$\eta1$			3.21	18.3	297.1	−16.6
					repulsion	
two BF_4		r_e(Li−B)		$\Delta E(r_e)$	total	Δ
$\eta2$	2.48			0.0	73.2	0.0
$\eta3$		2.31		5.1	77.3	4.2
$\eta1$			3.22	18.7	62.3	−10.9
three BF_4						
three $\eta2$	2.64			0.0		0.0
two $\eta2$ one $\eta1$	2.64		3.34	1.0		−10.2
four BF_4						
four $\eta1$			3.50	0.0		0.0
three $\eta1$ one $\eta2$	2.71		3.55	3.5		12.9
two $\eta1$ two $\eta2$	2.72		3.62	6.8		27.4

[a]The r_e values are in Å, while the relative energies are in kcal/mol. The structures are labelled by their coordination number, i.e., ηn means that n F atoms are interacting with the B atom. [b]The relative energies with each structure at equilibrium. [c]The relative energies when all structures use the Li−B distance of the $\eta2$ structure. [d]The relative energies when all structures use the Li−B distance of the $\eta1$ structure.

favorable Li^+−BF_4^- electrostatic interaction more for $\eta2$ than for $\eta1$.

As is clear from Figure 1, there is a change in BF_4^- orientation for $Li^+(BF_4^-)_4$ where all four ligands have an $\eta1$ orientation, resulting in T_d symmetry. For this system, we were able to find two additional minima: the first with three $\eta1$ ligands and one $\eta2$ ligand and the second with two $\eta1$ and two $\eta2$ ligands. The ligand−ligand repulsion for these two cases is larger than that for the most stable isomer. When four ligands are present, the ligand−ligand repulsion becomes the most important factor in determining the equilibrium structure. Note, for this system, the repulsion has become so important that the bond length of both the $\eta1$ and $\eta2$ ligands increases relative to the $Li^+(BF_4^-)_3$.

B. BF_4^-−BF_4^- Repulsion. As noted in the previous subsection, the BF_4^-−BF_4^- repulsion plays an important role in determining the optimal structure of the $Li^+(BF_4^-)_n$ systems. Therefore, we calibrate this repulsive interaction, which is computed as the energy of two BF_4^- ions as a function of the r(B−B) distance minus twice the energy of a single BF_4^- ion. In these calculations, the orientation of the two BF_4^- species is the same as that in $Li^+(BF_4^-)_2$, the B−B distance is fixed, and all other parameters are optimized. The exception to this procedure is the MP2 calculations in the aug-cc-pVQZ and aug-cc-pV5Z basis sets and the CCSD(T) calculations, where the geometric optimization is quite expensive, and therefore the MP2 aug-cc-pVTZ geometries are used. The plot of the potentials for the DFT functionals in the two different basis sets is compared with the $1/r$ electrostatic potential, the APPLE&P force field, and the traditional MP2 and CCSD(T) methods in Figure 2. Several facts are obvious from this plot: (1) For r values greater than about 6.5 Å, all of the potential curves, excluding the APPLE&P, are the same. (2) At r values less than 6.5 Å, the computed potentials are below the electrostatic potential because the molecules polarize away from each other, which reduces the repulsion. (3) At r values less than 5.5 Å, there is some small difference between the different methods. (4) The APPLE&P results differ somewhat from the other methods. Namely, in the 6−7 Å region, the APPLE&P results are below the other methods. From about 4.5 to 5.5 Å, the APPLE&P results are above the other methods, while at r values shorter than 4 Å the APPLE&P becomes increasingly less repulsive with decreasing r compared to the other methods.

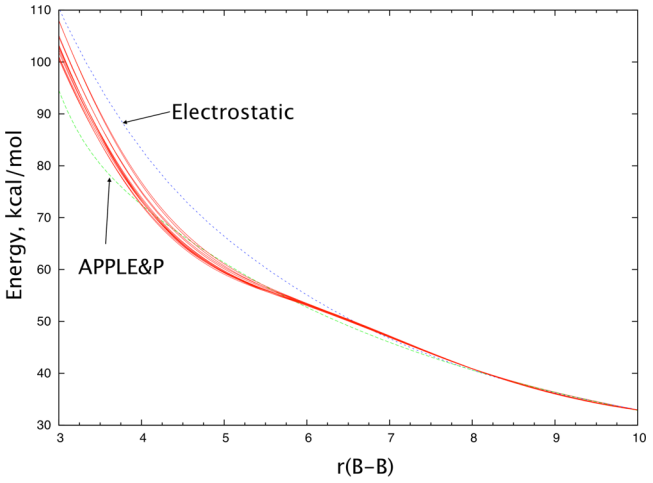

Figure 2. BF_4^-−BF_4^- interaction energy as a function of B−B distance. The $1/r$ electrostatic repulsion and the APPLE&P curves are labeled, while the remaining curves are the ab initio methods described in the text.

To quantify these differences, the energies are summarized for two r values, 5.7 and 4.0 Å, in Table 2. For the MP2 and CCSD(T) approaches, the change in interaction energy with basis set improvement is very small. Improving the basis set reduces the basis set superposition error (BSSE) that increases the repulsion but also introduces more polarization that can reduce the repulsion. These changes are as expected, and we extrapolate the CCSD(T) results to the complete basis set limit (CBS) using the aug-cc-pVTZ and aug-cc-pVQZ energies. At 5.7 Å, all of the methods are in good mutual agreement. At 4.0 Å, the difference between the different methods and between the two basis sets is larger. Now the largest error is 3.3 kcal/mol for the BPW91 approach in the small basis set. This error is more than 10 times that found at 5.7 Å.

dx.doi.org/10.1021/jp506422p | J. Phys. Chem. B 2014, 118, 10785−10794

Table 2. Summary of Results for BF_4^-−BF_4^- Interaction for r(B−B) Values of 5.7 and 4.0 Å, in kcal/mol

	r(B−B)			
	5.7		4.0	
	energy	ΔE	energy	ΔE
electrostatic	58.3	2.5	83.0	9.5
	6-31+G**			
B3LYP	56.0	0.2	75.0	1.5
B3LYP+D	55.7	0.0	72.6	−0.9
BPW91	56.0	0.3	76.8	3.3
PW91PW91	55.5	−0.2	73.9	−0.2
M05	55.8	0.0	73.2	−0.3
M06	55.9	0.1	74.7	1.2
M06L	56.1	0.3	74.1	0.6
	aug-cc-pVTZ			
B3LYP	55.9	0.1	74.8	1.3
B3LYP+D	55.6	−0.2	72.4	−1.1
BPW91	55.9	0.1	76.4	2.9
PW91PW91	55.4	−0.4	73.6	−0.4
M05	55.8	0.1	73.2	−0.3
M06	55.7	0.0	73.9	0.4
M06L	55.8	0.0	73.1	−0.5
MP2 aug-cc-pVTZ	55.6	−0.1	73.1	−0.4
MP2 aug-cc-pVQZ	55.7	−0.1	73.5	0.0
MP2 aug-cc-pV5Z	55.7	0.0	73.6	0.1
CCSD(T) aug-cc-pVTZ	55.6	−0.1	72.8	−0.7
CCSD(T) aug-cc-pVQZ	55.7	−0.1	73.2	−0.3
CCSD(T) CBS[a]	55.7	0.0	73.5	0.0
APPLE&P	55.1	−0.6	72.5	−1.1
APPLE&P(e44)	56.0	0.3	74.4	0.9

[a]The complete basis set limit as extrapolated from the CCSD(T) in the aug-cc-pVTZ and aug-cc-pVQZ basis sets.

Our molecular dynamical simulations[10] show that the BF_4^-−BF_4^- radial distribution function ($g(r)$) is extremely small for r values shorter than 5 Å at room temperature, and even at higher temperatures, $g(r)$ is very small at r values where the methods tested in this work differ. Therefore, the difference between the APPLE&P and other methods for describing the BF_4^-−BF_4^- interaction at short r is probably unimportant for most applications.

C. Li^+−BF_4^- Interaction. The first series of calibration calculations for Li^+−BF_4^- uses the MP2 and CCSD(T) approaches in conjunction with the cc-pV basis sets to study the η2, η3, and η1 configurations. The geometry is optimized at the MP2/cc-pVTZ level unless otherwise noted. The MP2 results as a function of basis set are shown in the top of Table 3. The cc-pVTZ basis set has a sizable BSSE of about 5 kcal/mol that varies somewhat with orientation. As expected, adding the diffuse functions (i.e., aug-cc-pVTZ) improves the description of the anion and reduces the BSSE by more than 4 kcal/mol. Expanding the basis set to aug-cc-pVQZ increases the binding energy and reduces the BSSE. The aug-cc-pV5Z reduces the BSSE slightly, and the binding energies hardly change compared with the aug-cc-pVQZ set. We compute the CBS limit for two choices of basis set and both with and without the BSSE correction. If the extrapolations were perfect, all four methods would yield the same results, and an inspection of the table shows that there is reasonable agreement between the CBS values. The best values are those obtained using the two largest basis sets.

We optimized the geometry at the MP2/aug-cc-pVTZ level and found a maximum difference of 0.03 kcal/mol compared with using the MP2/cc-pVTZ geometry. That is, the diffuse functions are needed to obtain accurate binding energies but are not needed to get reliable geometries.

We perform CCSD(T) calculations to see the effect of higher levels of correlation than found in the MP2. We find that the CCSD(T) results using the aug-cc-pVTZ basis set differ by a maximum of 0.29 kcal/mol from the MP2. Expanding the basis set to aug-cc-pVQZ increases the binding energy slightly, but the difference between the CCSD(T) and MP2 results in the aug-cc-pVQZ basis is similar to those in the aug-cc-pVTZ basis set. Clearly higher correlation is not very important in these electrostatically bound systems. Extrapolating the CCSD(T) results to the basis set limit yields very similar binding energies for the with and without BSSE correction results. We take the CCSD(T) CBS value as our best result.

Our best estimate for the Li^+−BF_4^- binding energy puts us in a position to evaluate the accuracy of the DFT approaches. We consider two basis sets and seven different functionals. The geometry is optimized for all combinations of basis set and functional. These DFT results are compared with our best estimate in Table 4. We report the average absolute difference, $|\bar{E}|$, between our DFT results and our best estimate. In the smaller 6-31+G** basis set, the B3LYP+D appears to be too strongly bound, while the BPW91, M06, and M06L are too weakly bound. The other three functionals agree with the best estimate to better than 1 kcal/mol. The results obtained using the large aug-cc-pVTZ basis paint a different picture; the three functionals that performed well in the small basis set, the B3LYP, PW91PW91, and M05, are now overbound by 2−3 kcal/mol. The best agreement with the CCSD(T) CBS value are for the M06 and M06L functionals. Our study of the $Li^+(BF_4^-)_n$ clusters showed that the η1 and η2 coordinations are probably the most important, and therefore, it is important that the difference in stability of these two coordinations be accurate. Excluding the B3LYP+D approach, this seems to be the case. The dispersion accounted for in the B3LYP+D increases with coordination, as expected, and therefore, the +D term stabilizes the η3 > η2 > η1.

The APPLE&P results are given at the bottom of Table 4. The APPLE&P yields similar binding energies for the η2 and η3 systems, which is consistent with all other methods; however, the APPLE&P has the η3 more stable than the η2. The η1 is less strongly bound than the other two configurations, as found at all other levels of theory. The difference between the APPLE&P results and our best estimate is larger than desirable. Borodin and co-workers[27] used the η1, η2, and η3 configurations in the development of the APPLE&P force field and noted the same limitations. This led to the development of a new version of the force field, denoted e44, and results using this version are also reported in Table 4. As can be seen, this version reduces the average error; the error in the η2 and η3 structures is reduced significantly, while the error in the η1 increases.

D. FSI and TFSI. We next consider the interaction of Li^+ with bis(trifluoromethane)sulfonimide anion, $(CF_3SO_2)_2N^-$, and bis(fluorosulfonyl)imide anion, $(FSO_2)_2N^-$; these anions are commonly called TFSI and FSI, respectively. At the B3LYP+D/6-31+G** level, the geometries of Li^+TFSI^- and Li^+FSI^- were optimized, and several local minima for each were found. Five optimized structures for Li^+TFSI^- are shown in Figure 3. In the first two TFSI configurations, the Li has an η2

dx.doi.org/10.1021/jp506422p | J. Phys. Chem. B 2014, 118, 10785−10794

Table 3. MP2 and CCSD(T) Calibration Calculations for $Li^+-BF_4^-$, in kcal/mol[a]

	cc-pV basis		binding energy			Δ-η2		
method	energy	geo	η1	η2	η3	η1	η2	η3
Effect of Basis Set Expansion on the MP2 Level at the cc-pVTZ Geometry								
MP2	TZ	TZ	129.39	147.65	146.28	18.26	0.00	1.37
BSSE	TZ	TZ	4.62	5.45	5.71			
MP2-BSSE	TZ	TZ	124.76	142.20	140.57	17.43	0.00	1.63
MP2	aug-TZ	TZ	125.06	142.21	140.56	17.15	0.00	1.65
BSSE	aug-TZ	TZ	0.44	0.80	0.85			
MP2-BSSE	aug-TZ	TZ	124.62	141.41	139.71	16.79	0.00	1.70
MP2	aug-QZ	TZ	125.82	142.71	140.83	16.88	0.00	1.87
BSSE	aug-QZ	TZ	0.28	0.42	0.46			
MP2-BSSE	aug-QZ	TZ	125.55	142.29	140.37	16.74	0.00	1.91
MP2	aug-5Z	TZ	125.84	142.69	140.79	16.86	0.00	1.90
BSSE	aug-5Z	TZ	0.16	0.24	0.24			
MP2-BSSE	aug-5Z	TZ	125.67	142.46	140.55	16.78	0.00	1.91
MP2	CBS(TZ,QZ)	TZ	126.38	143.07	141.03	16.69	0.00	2.04
MP2-BSSE	CBS(TZ,QZ)	TZ	126.22	142.93	140.86	16.71	0.00	2.06
MP2	CBS(5Z,QZ)	TZ	125.85	142.68	140.74	16.83	0.00	1.93
MP2-BSSE	CBS(5Z,QZ)	TZ	125.81	142.63	140.73	16.82	0.00	1.91
Effect of Optimizing the Geometry at the MP2/aug-cc-pVTZ Level								
MP2	aug-TZ	aug-TZ	125.09	142.23	140.57	17.13	0.00	1.66
MP2-BSSE	aug-TZ	aug-TZ	124.65	141.43	139.72	16.78	0.00	1.71
ΔMP2	aug-TZ	aug-TZ-TZ	0.03	0.02	0.01			
ΔMP2-BSSE	aug-TZ	aug-TZ-TZ	0.03	0.02	0.01			
Effect of Higher Levels of Correlation Treatment								
CCSD(T)	aug-TZ	TZ	125.25	142.50	140.84	17.26	0.00	1.67
BSSE	aug-TZ	TZ	0.46	0.86	0.91			
CCSD(T)-BSSE	aug-TZ	TZ	124.78	141.65	139.92	16.86	0.00	1.72
CCSD(T)-MP2	aug-TZ	TZ	0.18	0.29	0.28			
CCSD(T)-MP2-BSSE	aug-TZ	TZ	0.17	0.24	0.22			
CCSD(T)	aug-QZ	TZ	126.04	142.99	141.08	16.96	0.00	1.91
BSSE	aug-QZ	TZ	0.25	0.39	0.42			
CCSD(T)-BSSE	aug-QZ	TZ	125.78	142.61	140.66	16.82	0.00	1.95
CCSD(T)-MP2	aug-QZ	TZ	0.21	0.29	0.25			
CCSD(T)-MP2-BSSE	aug-QZ	TZ	0.24	0.32	0.28			
CCSD(T)	CBS	TZ	126.61	143.35	141.26	16.74	0.00	1.91
CCSD(T)-BSSE	CBS	TZ	126.51	143.31	141.19	16.79	0.00	1.95

[a]All geometries are taken from the MP2/cc-pVTZ or MP2/aug-cc-pVTZ sets, which are noted in the "geo" column.

coordination with the oxygen atoms in the TFSI, which can have a cis or trans configuration of the two CF_3 groups. The third structure has the Li with an η3 configuration. The last two structures have the Li coordinated with the central N atom with the TFSI having either a cis or trans configuration. We optimize the geometry and evaluate the binding energies using several other functionals in the small and large basis sets. We note that for many of the approaches the η3 structure collapses to an η2 structure. The binding energies of these five structures are given in Table 5. The order of the binding energies is η2 trans > η2 cis (>η3) > N trans > N cis. The four optimized structures for Li^+FSI^- are shown in Figure 4. They involve bridge or end-on bonding, with the FSI having either a cis or trans conformation. The bridge forms of Li^+FSI^- are more stable than the end-on forms. The cis confirmation is more stable than the trans for the bridge, but the trans is more stable for the end-on; see Table 5.

In addition to optimizing the MP2 geometry using the aug-cc-pVTZ set, we also perform the MP2 calculations using the B3LYP+D/6-31+G** geometry. The MP2 CBS limit is determined using the aug-cc-pVTZ and aug-cc-pVQZ basis sets. We note that using the fixed geometry introduces an error of less than 1 kcal/mol in the binding energies. This suggests that, when the MP2 geometry optimization is prohibitively expensive, the B3LYP+D geometry can be used with only a small loss in accuracy. Given the small effect of higher levels of correlation in $LiBF_4$ and the similar electrostatic bonding, we suspect that the MP2 CBS limit binding energies for Li^+-TFSI^- and Li^+-FSI^- are accurate. Using the MP2/aug-cc-pVTZ CBS values, we computed the average absolute error for the systems studied; note we do not include the η3 results when we compute the average absolute errors, since it is not a minimum at most levels. For the largest basis set, the smallest errors are for BPW91 and M06L. The error for the M06 is only slightly larger. For the small basis set, five functionals have errors of less than 2.5 kcal/mol.

The APPLE&P results for TFSI and FSI using the B3LYP+D/6-31+G** geometries are in good agreement with the MP2 CBS values. For TFSI, the APPLE&P force field correctly places the η2 trans and η2 cis very close in energy, with the η3 and N bonding cases higher in energy. For FSI, the APPLE&P force field correctly finds the bridge to be more stable than the end-on, but the trans conformation of the FSI is slightly below the cis. The bridge binding energies are in very good agreement with the MP2 CBS values. The average absolute error for the

dx.doi.org/10.1021/jp506422p | J. Phys. Chem. B 2014, 118, 10785−10794

Table 4. Summary of DFT Calibration Calculations, in kcal/mol, for $Li^+-BF_4^-$ [a]

	binding energy			BE-best			
	$\eta1$	$\eta2$	$\eta3$	$\eta1$	$\eta2$	$\eta3$	$\lvert\bar{E}\rvert$
			Small Basis Set				
B3LYP	125.7	142.4	139.9	−0.9	−1.0	−1.3	1.1
B3LYP+D	126.7	145.6	144.5	0.1	2.3	3.3	1.9
BPW91	122.9	139.4	137.8	−3.8	−3.9	−3.5	3.7
PW91PW91	125.3	142.4	140.7	−1.3	−1.1	−0.5	0.9
M05	126.0	142.4	140.1	−0.6	−1.0	−1.1	0.9
M06	123.9	140.2	138.4	−2.7	−3.2	−2.9	2.9
M06L	124.5	141.6	140.0	−2.2	−1.8	−1.3	1.7
			aug-cc-pVTZ Set				
B3LYP	128.3	145.2	143.0	1.7	1.8	1.7	1.7
B3LYP+D	129.2	148.3	147.1	2.6	5.0	5.8	4.5
BPW91	125.3	142.2	140.8	−1.3	−1.1	−0.5	1.0
PW91PW91	128.0	145.4	144.1	1.3	2.1	2.8	2.1
M05	129.2	146.2	144.4	2.6	2.8	3.1	2.9
M06	126.6	143.2	141.6	0.0	−0.2	0.3	0.2
M06L	126.9	143.6	142.1	0.3	0.2	0.9	0.5
BEST	126.6	143.4	141.3	0.0	0.0	0.0	0.0
APPLE&P	126.0	147.4	149.0	−0.6	4.1	7.7	
APPLE&P(e44)	122.2	141.6	142.3	−4.5	−1.8	1.0	

[a]The DFT geometry is optimized for each functional and basis set. The "best" results are the extrapolated CCSD(T) calculations from the previous table. The APPLE&P force field results are also included for comparison.

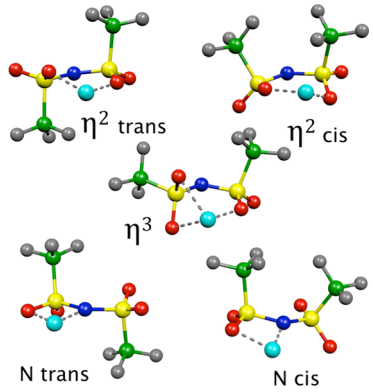

Figure 3. B3LYP+D/6-31+G** optimized geometries for the Li^+TFSI^- structures considered in this work.

APPLE&P results is smaller than many of the DFT functionals even in the largest basis set. For TFSI, optimizing the geometry at the APPLE&P level improves the agreement for the N bonding cases but leads to an overbinding of the $\eta2$ trans and $\eta2$ cis cases. The $\eta3$ structure collapses to the $\eta2$ trans structure, as found for many of the DFT approaches. For FSI, optimizing the APPLE&P geometry slightly increases the bridge binding energies while significantly increasing the end-on binding energies. While the bridge binding APPLE&P geometries are very similar to those obtained with the DFT approaches, the end-on APPLE&P geometries are $\eta1$ instead of the $\eta2$ configuration found at the DFT level; see Figure 4. Starting from the APPLE&P $\eta1$ trans geometry, all seven of the functionals in the 6-31+G** basis set, when optimized, return to the end-on $\eta2$ configuration. The APPLE&P clearly yields reasonable binding energies, but there are some differences between APPLE&P and DFT approaches with respect to the geometries of some of the complexes.

In Figure 5, the Li^+-TFSI^- potential is reported. We report the potential where all parameters except the Li−TFSI center of mass (CM) distance have been optimized and a potential where the TFSI geometry is fixed at that of isolated $TFSI^-$ and only the Li−CM has been varied. In addition to the computed potentials, the electrostatic potential is plotted. This is computed as $-1/r + \mu/r^2$, where μ is the dipole moment of $TFSI^-$ computed at the CM and r is the distance between the Li^+ and the $TFSI^-$ CM, scaled by 1.00866. The scale factor brings the computed potential into agreement with the electrostatic potential at 10.444 Å. Both of the computed potentials fall below the electrostatic potential, which includes the charge−charge and charge−dipole terms at about 6 Å due to polarization of the two fragments. As the Li−CM distance decreases, the polarization increases and the difference between the computed potentials and the electrostatic potential increases. This continues until the charge distributions of the two fragments begin to overlap at short distances, which leads to a repulsion between the Li^+ and $TFSI^-$, that results in the computed potentials rising above the electrostatic potential, which includes only attractive terms. For the fixed geometries, the APPLE&P and B3LYP potentials are very similar. When the TFSI geometry is allowed to relax, the binding energy increases as expected, but the APPLE&P potential becomes somewhat broader than the B3LYP results. The results presented for Li^+-TFSI^- are expected to be typical of Li^+−anion systems. The difference between the electrostatic and computed potentials will depend on the polarizability of the anion, which affects the size of the charge-induced dipole term. In this regard, we note that McOwen et al.[28] suggested reducing the polarizability of oxygen in the APPLE&P force field. They proposed this to decrease the Li^+-TFSI^- binding energy, thus bringing it into better agreement with more accurate calculations. This should also make the APPLE&P potential somewhat less broad, which would also be consistent with the calculations performed in this work.

dx.doi.org/10.1021/jp506422p | J. Phys. Chem. B 2014, 118, 10785−10794

Table 5. Comparison of the Results (in kcal/mol) for Li^+TFSI^- and Li^+FSI^- as a Function of the Basis Set and Method Used[a]

		TFSI					FSI				
method	basis	η2 T	η2 C	η3	N T	N C	bridge T	end-on T	bridge C	end-on C	$\lvert\bar{E}\rvert$
B3LYP	6-31+G**	139.6	138.5	*b*	129.9	129.2	135.8	118.6	137.1	118.2	2.0
B3LYP+D	6-31+G**	144.2	143.8	138.7	133.7	133.3	139.9	121.4	140.7	120.9	4.9
BPW91	6-31+G**	135.3	133.9	*b*	127.5	126.9	131.5	115.7	132.2	115.3	3.0
PW91PW91	6-31+G**	138.6	137.7	*b*	130.6	130.0	135.1	118.6	135.9	118.3	2.1
M05	6-31+G**	139.2	138.3	133.1	129.4	128.9	135.6	119.0	137.0	118.5	1.7
M06	6-31+G**	136.3	135.4	*b*	126.7	126.3	133.2	116.6	133.9	116.0	2.1
M06L	6-31+G**	135.8	135.1	130.5	127.0	126.8	132.6	116.3	133.4	115.8	2.3
B3LYP	aug-cc-pVTZ	141.7	140.5	*b*	130.3	129.6	138.9	122.1	140.4	121.7	3.3
B3LYP+D	aug-cc-pVTZ	146.3	145.9	140.8	134.2	133.6	142.7	124.7	144.0	124.2	7.1
BPW91	aug-cc-pVTZ	137.3	136.0	*b*	128.1	127.4	134.4	119.3	135.6	119.0	1.1
PW91PW91	aug-cc-pVTZ	140.9	139.9	*b*	131.4	130.7	138.1	122.5	139.4	122.1	3.3
M05	aug-cc-pVTZ	142.5	141.7	137.0	131.3	130.9	139.9	123.7	141.5	123.2	4.5
M06	aug-cc-pVTZ	139.5	138.7	*b*	128.6	128.2	136.8	120.8	138.3	120.3	1.6
M06L	aug-cc-pVTZ	138.7	138.1	*b*	128.4	128.2	136.2	120.2	137.8	119.8	1.1
MP2	aug-cc-pVTZ	136.7	135.9	*b*	127.3	126.7	135.0	119.4	136.4	118.9	0.7
MP2[c]	aug-cc-pVQZ	136.8	135.8	*b*	126.4	126.9	135.4	119.9	137.2	119.4	0.3
MP2[c]	CBS	136.8	135.8	*b*	125.7	127.1	135.8	120.2	137.7	119.8	0.0
MP2[d]	aug-cc-pVTZ	135.7	135.1	131.7	127.2	126.7	134.7	119.2	136.3	118.7	1.0
MP2[d]	aug-cc-pVQZ	135.6	135.0	131.2	126.9	126.4	135.0	119.5	137.0	119.1	0.8
MP2[d]	CBS	135.6	134.9	130.7	126.6	126.1	135.2	119.8	137.5	119.4	0.7
APPLE&P[d]		135.1	134.7	128.8	122.2	121.4	136.2	113.1	135.6	112.5	3.6
APPLE&P		140.4	140.5	*b*	126.7	126.4	139.0	122.3	138.3	122.3	2.3

[a]The geometry is fully optimized at each level of theory unless otherwise noted. "T" signifies the trans conformation of FSI or TFSI, while "C" signifies the cis conformation. [b]Collapsed to η2 trans when optimized. [c]The geometry is taken from the MP2/aug-cc-pVTZ calculation. [d]The geometry is taken from the B3LYP+D/6-31+G** calculation.

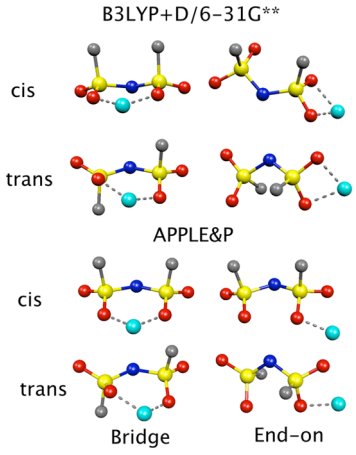

Figure 4. APPLE&P and B3LYP+D/6-31+G** optimized geometries for the Li^+FSI^- structures considered in this work.

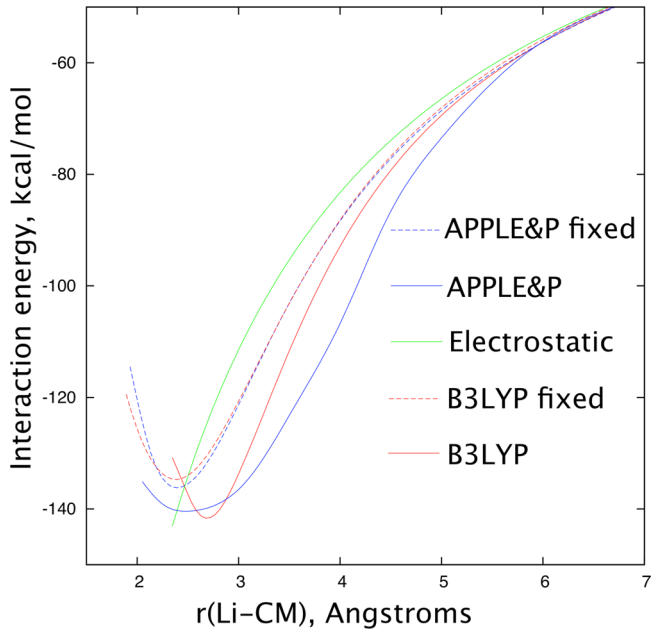

Figure 5. Comparison of the APPLE&P and B3LYP/aug-ccpVTZ potentials for the Li^+–$TFSI^-$ center of mass (CM) distance. Also given is the electrostatic potential that includes the charge–charge and charge–dipole terms.

The final set of calibration calculations are for the $Li^-(FSI^-)_2$ and $Li^-(TFSI^-)_2$ systems. For $Li^-(FSI^-)_2$, we find three interesting minima, which are shown in Figure 6. All of the structures have η2 coordination for each ligand; in one, the bonding of both ligands is end-on to the Li^+, while, in the other two, the Li^+ bridges both FSI anions. These two bridge binding structures differ in the conformation of the FSI anions; in one they are both cis, while in the other they are both trans. The binding energies are summarized in Table 6. The binding energies are bridge cis > bridge trans > end-one trans. This is consistent with the results found for the Li^+FSI^-. Our best value is the MP2 result extrapolated to the CBS limit. The average absolute error is reported for all methods and compared with the MP2 CBS values. For the small basis set, we find the B3LYP, PW91PW91, and M05 functionals agree very well with our best results. In the aug-cc-pVTZ basis set, the best functionals are B3LYP, PW91PW91, M06, and M06L. It is interesting that the B3LYP and PW91PW91 are among the best for both basis sets. The APPLE&P results using the MP2/aug-cc-pVTZ geometry have an average absolute error of 5.7 kcal/

dx.doi.org/10.1021/jp506422p | J. Phys. Chem. B 2014, 118, 10785–10794

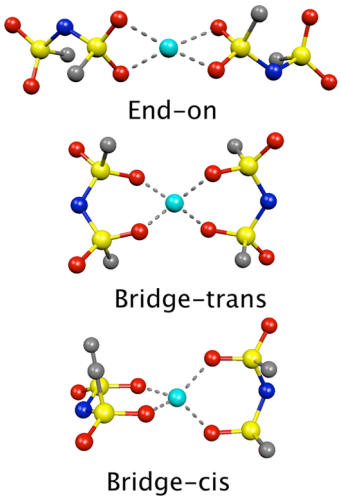

Figure 6. B3LYP+D/aug-ccpVTZ optimized geometries for the $Li^+(FSI^-)_2$ considered in this work.

mol, which is reduced to 2.6 kcal/mol when the structures are optimized. While the optimization increases the binding energy of the bridges by 2.5 and 3.1 kcal/mol, it increases the binding of the end-on by 14.4 kcal/mol. An inspection of the APPLE&P optimized geometries shows only small changes for the bridge structure, but the end-one changes from $\eta 2$ for both ligands to $\eta 1$ for both ligands.

The $Li^+(TFSI^-)_2$ results are summarized Table 7. For this system, it would be very difficult to optimize the geometry at the MP2 level using the aug-cc-pVTZ basis set. The Li^+TFSI^- and Li^+FSI^- results in Table 5 show that using the B3LYP+D/6-31+G* geometry instead of the MP2/aug-cc-pVTZ geometry yields an average absolute error of 0.7 kcal/mol. We therefore use the DFT geometry for the MP calculations. In this case, we use three different DFT geometries, namely, the B3LYP+D/6-31+G**, B3LYP+D/aug-cc-pVTZ, and B3LYP/aug-cc-pVTZ geometries. The MP2 binding energies using the B3LYP+D/6-

Table 7. Comparison of Results (in kcal/mol) for $Li^+(TFSI^-)_2$ as a Function of Basis Set and Method[a]

	BE		BE-best		
	end-on	bridge	end-on	bridge	$\|\bar{E}\|$
B3LYP/6-31+G**	164.5	184.5	0.4	−1.0	0.7
B3LYP+D/6-31+G**	174.2	195.0	10.1	9.5	9.8
BPW91/6-31+G**	159.6	176.3	−4.5	−9.2	6.9
PW91PW91/6-31+G**	165.5	184.0	1.3	−1.6	1.4
M05/6-31+G**	166.7	187.0	2.6	1.4	2.0
M06/6-31+G**	161.9	183.0	−2.2	−2.6	2.4
M06L/6-31+G**	161.8	182.5	−2.3	−3.0	2.7
B3LYP/aug-cc-pVTZ	165.0	184.9	0.9	−0.6	0.7
B3LYP+D/aug-cc-pVTZ	174.7	195.1	10.6	9.5	10.1
BPW91/aug-cc-pVTZ	160.4	177.0	−3.7	−8.6	6.2
PW91PW91/aug-cc-pVTZ	166.3	184.5	2.1	−1.1	1.6
M05/aug-cc-pVTZ	168.9	189.0	4.8	3.4	4.1
M06/aug-cc-pVTZ	164.1	185.3	0.0	−0.3	0.2
M06L/aug-cc-pVTZ	163.3	185.0	−0.8	−0.5	0.7
MP2/aug-cc-pVTZ[b]	164.0	184.8	−0.1	−0.7	0.4
MP2/aug-cc-pVTZ[c]	164.2	185.4	0.1	−0.1	0.1
MP2/aug-cc-pVTZ[d]	164.1	185.6	0.0	0.0	0.0
APPLE&P	169.9	183.3	5.8	−2.3	4.0

[a]The geometry is fully optimized at each level of theory unless otherwise noted. [b]The geometry is taken from the B3LYP/aug-cc-pVTZ calculation. [c]The geometry is taken from the B3LYP+D/6-31+G** calculation. [d]The geometry is taken from the B3LYP+D/aug-cc-pVTZ calculation.

Table 6. Comparison of Results (in kcal/mol) for $Li^+(FSI^-)_2$ as a Function of Basis Set and Method[a]

	BE			BE-best			
	end-on T	bridge T	bridge C	end-on T	bridge T	bridge C	$\|\bar{E}\|$
B3LYP/6-31+G**	162.4	180.3	182.1	−1.6	−0.7	−1.2	1.2
B3LYP+D/6-31+G**	171.2	189.5	190.1	7.2	8.5	6.8	7.5
BPW91/6-31+G**	157.0	172.3	173.5	−7.0	−8.8	−9.8	8.5
PW91PW91/6-31+G**	162.8	179.6	180.9	−1.2	−1.4	−2.4	1.7
M05/6-31+G**	164.7	182.7	184.6	0.7	1.7	1.3	1.2
M06/6-31+G**	159.9	178.3	179.2	−4.1	−2.8	−4.1	3.7
M06L/6-31+G**	159.5	177.6	178.5	−4.5	−3.5	−4.8	4.2
B3LYP/aug-cc-pVTZ	164.8	182.0	184.2	0.8	1.0	0.9	0.9
B3LYP+D/aug-cc-pVTZ	173.6	190.9	192.3	9.6	9.9	8.9	9.5
BPW91/aug-cc-pVTZ	159.6	174.1	175.9	−4.4	−7.0	−7.4	6.2
PW91PW91/aug-cc-pVTZ	165.4	181.3	183.2	1.4	0.3	−0.1	0.6
M05/aug-cc-pVTZ	168.8	186.0	188.2	4.8	5.0	4.9	4.9
M06/aug-cc-pVTZ	163.7	181.2	182.8	−0.3	0.2	−0.5	0.3
M06L/aug-cc-pVTZ	163.0	181.0	182.8	−1.0	0.0	−0.5	0.5
MP2/aug-cc-pVTZ	164.0	181.8	183.3	0.0	0.8	0.0	0.3
MP2/aug-cc-pVQZ[b]	164.0	181.3	183.3	0.0	0.3	0.0	0.1
CBS[b]	164.0	181.0	183.3	0.0	0.0	0.0	0.0
APPLE&P[b]	154.8	178.3	178.0	−9.1	−2.7	−5.3	5.7
APPLE&P	169.2	180.8	181.1	5.2	−0.2	−2.3	2.6

[a]The geometry is fully optimized at each level of theory unless otherwise noted. "T" signifies the trans conformation of FSI or TFSI, while "C" signifies the cis conformation. [b]The MP2/aug-cc-pVTZ geometry is used.

dx.doi.org/10.1021/jp506422p | J. Phys. Chem. B 2014, 118, 10785−10794

31+G** or B3LYP+D/aug-cc-pVTZ geometries were very similar, while the MP2 binding energies obtained using the B3LYP/aug-cc-pVTZ geometry were smaller. The MP2 results at the B3LYP+D/aug-cc-pVTZ geometry had the largest binding energy and are taken as our best value, and therefore, the other methods are compared with them. In the small basis set, the B3LYP and M05 have errors of 2 kcal/mol or less, while, in the bigger basis set, the B3LYP, PW91PW91, M06, and M06L functionals have average absolute errors smaller than 2 kcal/mol. The APPLE&P is in reasonable agreement with our best estimates. As found in other cases, the APPLE&P optimal geometry for the end-on orientation shows the same change from $\eta 2$ to $\eta 1$ bonding compared with the DFT approaches. As for the other systems, the bridge bonding cases have geometries that are similar to that obtained by the DFT approaches.

E. Comparison of Systems. A summary of the errors for all of the systems considered is reported in Table 8. The

Table 8. Summary of the Average Absolute Errors (in kcal/mol) for the Different Functionals in the Two Basis Sets[a]

	$Li^+-(T)FSI^-$		$Li^+-(FSI^-)_2$		$Li^+-(TFSI^-)_2$	
	small	big	small	big	small	big
B3LYP	2.6	3.3	1.2	0.9	0.7	0.7
B3LYP+D	4.9	7.1	7.5	9.5	9.8	10.1
BPW91	3.0	1.1	8.5	6.2	6.9	6.2
PW91PW91	2.1	3.3	1.7	0.6	6.9	1.6
M05	1.7	4.5	1.2	4.9	2.0	4.1
M06	2.1	1.6	3.7	0.3	2.4	0.2
M06L	2.3	1.1	4.2	0.5	2.7	0.7
APPLE&P	2.8		2.6		4.0	
	$BF_4^--BF_4^-$		$Li^+-BF_4^-$		all	
	small	big	small	big	small	big
B3LYP	1.5	1.3	1.1	1.7	2.6	3.3
B3LYP+D	0.9	1.2	1.9	4.5	9.8	10.1
BPW91	3.3	2.9	3.7	1.0	8.5	6.2
PW91PW91	0.2	0.4	0.9	2.1	6.9	3.3
M05	0.3	0.3	0.9	2.9	2.0	4.9
M06	1.2	0.4	2.9	0.2	3.7	1.6
M06L	0.6	0.5	1.7	0.5	4.2	1.1
APPLE&P	1.1		4.2		4.2	

[a]The APPLE&P is also reported.

performance of the methods depends on the basis set, as expected. Four of the methods have average absolute errors of less than 3 kcal/mol for all of the systems considered. These are the B3LYP and M05 in the small basis set and the M06 and M06L in the larger basis set. Overall, the M06L in the large basis set has the smallest errors. Previous work[29−31] also concluded that the M06L is the functional that is in the best agreement with higher levels of theory. We should also note that the geometry optimization of the M06L routinely required fewer steps than the M06 optimization, which is an additional reason favoring the M06L over the M06.

Adding the dispersion in the B3LYP+D approach increases the binding energy, which increases the error compared to the B3LYP approach. This implies that there is some cancellation of errors in the B3LYP approach, since it has a smaller error even though it does not include dispersion. However, the MP2 energies for the $Li^+-(TFSI^-)_2$ systems suggest that the B3LYP+D geometries may be superior to those at the B3LYP level despite the overbinding. It is interesting to note that some functionals show a significant variation in performance. For example, the BPW91 in the large basis set does very well for $Li^+-BF_4^-$ and $Li^+-(T)FSI^-$ but has a significant error for the cases with two anions, namely, $BF_4^--BF_4^-$ and $Li^+-((T)-FSI^-)_2$. Presumably the anion−anion interaction is not as well described as the cation−anion interaction. The errors for PW91PW91 in the large basis set suggest the opposite performance, where the cases with two anions perform better than those with only one anion. The APPLE&P performs reasonably well compared with the DFT approaches. While the APPLE&P yields binding energies that are in good agreement with the most accurate calculations, the finer points, such as the energy difference between different isomers, can be less reliable. For example, the APPLE&P has the $\eta 3$ orientation of $Li^+-BF_4^-$ as the most stable, while all other methods have the $\eta 2$ as the most stable. For two TFSI or two FSI anions, the APPLE&P appears to reduce the difference in energy between the end-on and bridge configurations. Associated with the reduction in energy is a change in configuration for the APPLE&P, which yields an $\eta 1$ configuration, while the DFT yields $\eta 2$ in some cases. However, we note that this change in geometry is not for the most stable isomer.

IV. CONCLUSIONS

For $BF_4^--BF_4^-$ and $Li^+-BF_4^-$, we are able to extrapolate the CCSD(T) calculations to the complete basis set limit. The CBS MP2 results are in excellent agreement with the CBS CCSD(T) values. For the Li^+ interaction with one or two FSI and TFSI anions, the CCSD(T) calculations are not practical and only MP2 calculations are performed. On the basis of the results for the BF_4 systems, we believe that the MP2 results are still very reliable for the FSI and TFSI systems as well. We compare our best results to DFT results obtained using two basis sets and a variety of functionals. Overall, the B3LYP and M05 functionals appear to be the best choice for the small basis set, while the M06 and M06L functionals are the best choice for the large basis set. While the errors are very similar for the M06 and M06L functionals, the M06L seems to optimize the geometry in fewer steps than the M06, and therefore is the method of choice in the large basis set. The APPLE&P is in reasonable agreement with our best calculations, and in many cases, it outperforms some of the DFT functionals.

■ ASSOCIATED CONTENT

Supporting Information

The geometries and total energies of the $Li(BF)_4$, LiTFSI, $Li(TFSI)_2^-$, LiFSI, and $Li(FSI)_2^-$ molecules for the M06L/aug-cc-pVTZ level of theory. A LAMMPS input for $LiBF_4$ using the e44 force field is also included. This material is available free of charge via the Internet at http://pubs.acs.org.

■ AUTHOR INFORMATION

Corresponding Author

*E-mail: Charles.W.Bauschlicher@nasa.gov.

Notes

The authors declare no competing financial interest.

[†]C.W.B.: Mail Stop 230-3, Entry Systems and Technology Division.

[‡]J.B.H., E.W.B., J.W.L.: Mail Stop 234-1, Thermal Protection Materials Branch.

■ ACKNOWLEDGMENTS

This work was supported by funding from the NASA Aeronautics Research Institute Seedling program.

■ REFERENCES

(1) Schweikert, N.; Hofmann, A.; Schulz, M.; Scheuermann, M.; Boles, S. T.; Hanemann, T.; Hahn, H.; Indris, S. Suppressed lithium dendrite growth in lithium batteries using ionic liquid electrolytes: Investigation by electrochemical impedance spectroscopy, scanning electron microscopy, and in situ ^{7}Li nuclear magnetic resonance spectroscopy. *J. Power Sources* **2013**, *228*, 237−243.

(2) Bhattacharyya, R.; Key, B.; Chen, H.; Best, A. S.; Hollenkamp, A. F.; Grey, C. P. *In situ* NMR observation of the formation of metallic lithium microstructures in lithium batteries. *Nat. Mater.* **2010**, *9*, 504−510.

(3) Borodin, O.; Gorecki, W.; Smith, G. D.; Armand, M. Molecular Dynamics Simulations and Pulsed-Field Gradient NMR Studies of Bis(fluorosulfonyl)imide (FSI) and Bis[trifluoromethyl)sulfonly]imid (TFSI)-Based Ionic Liquids. *J. Phys. Chem. B* **2010**, *114*, 6786−6798.

(4) Borodin, O.; Smith, G. D. Development of Many-Body Polarizable Force Fields for Li-Battery applications: 2. LiTFSI-Doped Oligoether, Polyether, and Carbonate-Based Electrolytes. *J. Phys. Chem. B* **2006**, *110*, 6293−6299.

(5) Lassegues, J. C.; Grondin, J.; Aupetit, C.; Johansson, P. Spectroscopic Identification of the Lithium Ion Transporting Species in LiTFSI-Doped Ionic Liquids. *J. Phys. Chem. A* **2009**, *113*, 305−314.

(6) Johansson, P.; Gejji, S. P.; Tegenfeldt, J.; Lindgren, J. The imide ion: potential energy surface and geometries. *Electrochim. Acta* **1998**, *43*, 1375−1379.

(7) Gejji, S. P.; Suresh, C. H.; Babu, K.; Gadre, S. R. Ab Initio Structure and Vibrational Frequencies of $(CF_3SO_2)_2N^-Li^+$ Ion Pairs. *J. Phys. Chem. A* **1999**, *103*, 7474−7480.

(8) Fujii, K.; Hamano, H.; Doi, H.; Song, X.; Tsuzuki, S.; Hayamizu, K.; Seki, S.; Kameda, Y.; Dokko, K.; Watanabe, M.; Umebauashi, Y. Unusual Li^+ Ion Solvation Structure in Bis(fluorosulfonyl)amide Based Ionic Liquid. *J. Phys. Chem. C* **2013**, *117*, 19314−19324.

(9) Borodin, O. Polarizable Force Field Development and Molecular Dynamics Simulations of Ionic Liquids. *J. Phys. Chem. B* **2009**, *113*, 11463−11478.

(10) Haskins, J. B.; Wu, J. J.: Hernandez, D. M.; Bennett, W. R.; Borodin, O.; Monk, J. D.; Bauschlicher, C. W.; Lawson, J. W. Computational and Experimental Investigation of Li-doped Ionic Liquid Electrolytes: [pyr14][TFSI], [pyr13][FSI], and [EMIM][BF4]. *J. Phys. Chem. B*, in press, DOI: 10.1021/jp5061705.

(11) Becke, A. D. Density-functional thermochemistry. III. The role of exact exchange. *J. Chem. Phys.* **1993**, *98*, 5648−5652.

(12) Stephens, P. J.; Devlin, F. J.; Chabalowski, C. F.; Frisch, M. J. Ab initio Calculation of Vibrational Absorption and Circular Dichroism Spectra Using Density Functional Force Fields. *J. Phys. Chem.* **1994**, *98*, 11623−11627.

(13) Grimme, S. Semiempirical GGA-type density functional constructed with a long-range dispersion correction. *J. Comput. Chem.* **2006**, *27*, 1787−1799.

(14) Becke, A. D. Density-functional exchange-energy approximation with correct asymptotic-behavior. *Phys. Rev. A* **1988**, *38*, 3098−3100.

(15) Perdew, J. P.; Burke, K.; Wang, Y. Generalized gradient approximation for the exchange-correlation hole of a many-electron system. *Phys. Rev. B* **1996**, *54*, 16533−16539.

(16) Zhao, Y.; Schultz, N. E.; Truhlar, D. G. Exchange-correlation functional with broad accuracy for metallic and nonmetallic compounds, kinetics, and noncovalent interactions. *J. Chem. Phys.* **2005**, *123*, 161103 (1−3).

(17) Zhao, Y.; Truhlar, D. G. The M06 suite of density functionals for main group thermochemistry, thermochemical kinetics, noncovalent interactions, excited states, and transition elements: two new functionals and systematic testing of four M06-class functionals and 12 other functionals. *Theor. Chem. Acc.* **2008**, *120*, 215−241.

(18) Zhao, Y.; Truhlar, D. G. A new local density functional for main-group thermochemistry, transition metal bonding, thermochemical kinetics, and noncovalent interactions. *J. Chem. Phys.* **2006**, *125*, 194101 (1−18).

(19) Bartlett, R. J. Many-Body Perturbation Theory and Coupled Cluster Theory for Electron Correlation in Molecules. *Annu. Rev. Phys. Chem.* **1981**, *32*, 359−401.

(20) Raghavachari, K.; Trucks, G. W.; Pople, J. A.; Head-Gordon, M. A fifth-order perturbation comparison of electron correlation theories. *Chem. Phys. Lett.* **1989**, *157*, 479−483.

(21) Frisch, M. J.; Pople, J. A.; Binkley, J. S. Self-Consistent Molecular Orbital Methods. 25. Supplementary Functions for Gaussian Basis Sets. *J. Chem. Phys.* **1984**, *80*, 3265−3269 and references therein.

(22) Dunning, T. H. Gaussian basis sets for use in correlated molecular calculations. I. The atoms boron through neon and hydrogen. *J. Chem. Phys.* **1989**, *90*, 1007−1023.

(23) Kendall, R. A.; Dunning, T. H.; Harrison, R. J. Electron affinities of the first-row atoms revisited. Systematic basis sets and wave functions. *J. Chem. Phys.* **1992**, *96*, 6796−6806.

(24) Helgaker, T.; Klopper, W.; Koch, H.; Noga, J. Basis-set convergence of correlated calculations on water. *J. Chem. Phys.* **1997**, *106*, 9639−9646.

(25) Frisch, M. J.; et al. *Gaussian 09*, revision C.01; Gaussian, Inc.: Pittsburgh, PA, 2009.

(26) Plimpton, S. J. Fast Parallel Algorithms for Short-Range Molecular Dynamic. *Comput. Phys.* **1995**, *117*, 1−19 (http://lammps.sandia.gov).

(27) Borodin, O.; Smith, G. D.; Douglas, R. Force Field Development and MD Simulations of Poly(ethylene oxide)/$LiBF_4$ Polymer Electrolytes. *J. Phys. Chem. B* **2003**, *107*, 6824−6837.

(28) McOwen, D. W.; Seo, D. M.; Borodin, O.; Vatamanu, J.; Boyle, P. D.; Henderson, W. A. Concentrated electrolytes: decrypting electrolyte properties and reassessing Al corrosion mechanisms. *Energy Environ. Sci.* **2014**, *7*, 416−426.

(29) Borodin, O.; Zhuang, G. V.; Ross, P. N.; Xu, K. Molecular Dynamics Simulations and Experimental Study of Lithium Transport in Dilithium Ethylene Dicarbonate. *J. Phys. Chem. C* **2013**, *117*, 7433−7444.

(30) Han, S.-D.; Borodin, O.; Allen, J. L.; Seo, D. M.; McOwen, D. W.; Yun, S.-H.; Henderson, W. A. Electrolyte Solvation and Ionic Association: IV. Acetonitrile-Lithium Difluoro(oxalato)borate (LiDFOB) Mixtures. *J. Electrochem. Soc.* **2013**, *160*, A2100−A2110.

(31) Bryantsev, V. Calculation of Solvation Free Energies of Li^+ and O_2^- Ions and Neutral Lithium-Oxygen Compounds in Acetonitrile Using Mixed Cluster/Continuum Methods. *Theor. Chem. Acc.* **2012**, *131*, 1250(1−11).